

Supplementary Information

**Ancestral neural circuits potentiate the origin of a female sexual behavior in *Drosophila***

Minhao Li<sup>1</sup>, Dawn S. Chen<sup>1</sup>, Ian P. Junker<sup>1</sup>, Fabianna I. Szorenyi<sup>1</sup>, Guan Hao Chen<sup>1</sup>, Arnold J. Berger<sup>1</sup>, Aaron A. Comeault<sup>2,3</sup>, Daniel R. Matute<sup>2</sup>, Yun Ding<sup>1\*</sup>

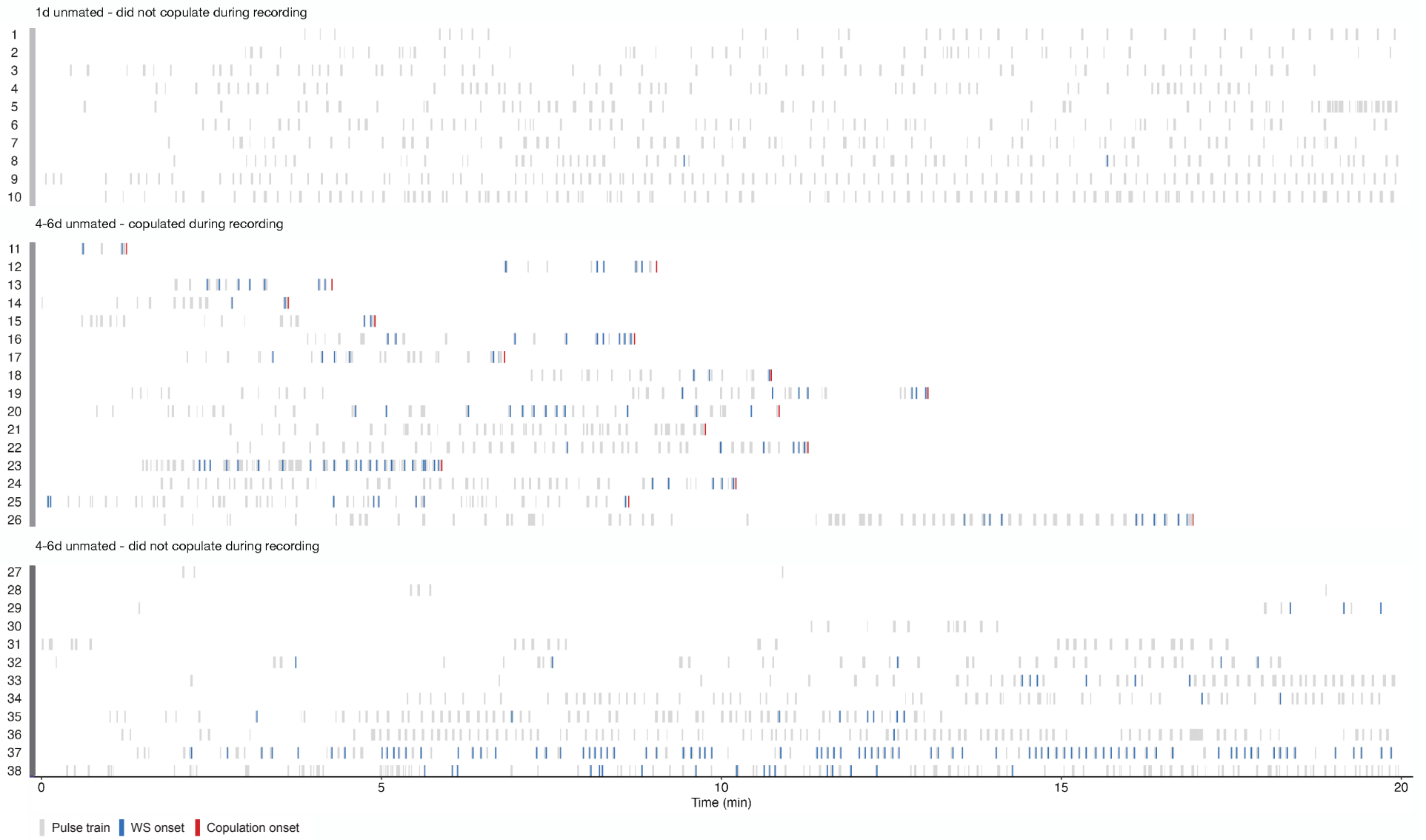
These authors contributed equally: Minhao Li, Dawn S. Chen

Corresponding author: correspondence to Yun Ding (yding19@sas.upenn.edu)

<sup>1</sup>Department of Biology, University of Pennsylvania, Philadelphia, PA, USA

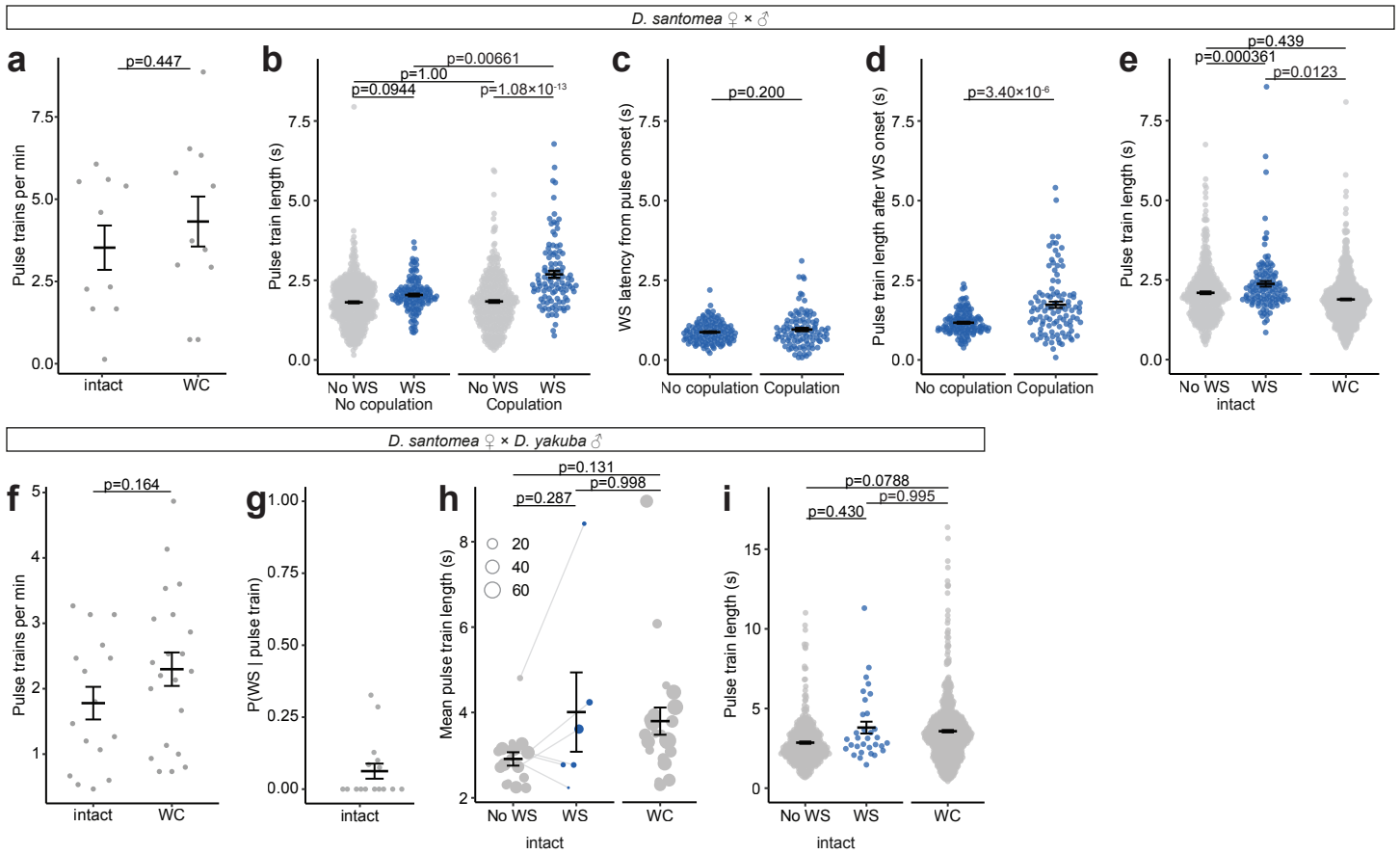
<sup>2</sup>Department of Biology, University of North Carolina, Chapel Hill, NC, USA

<sup>3</sup>Current address: School of Environmental and Natural Sciences, Bangor University, Bangor, UK



**Supplementary Fig. 1: Full-length behavioral ethograms of *D. santomea* courting pairs.**

Each row corresponds to one courting pair, with the numbers to the left representing their pair ID. n=38. Source data are provided as a Source Data file.



**Supplementary Fig. 2: Additional behavioral analyses linked to Fig. 2 showing wing spreading-dependent modulation of pulse train length in conspecific pairs and its absence in heterospecific pairs.**

**a**, Number of pulse trains per minute that males produced when paired with intact or wing-cut (WC) females. Only data from pairs that did not copulate during the recording period are shown.  $n=10, 11$ .

**b**, Length of pulse trains separated by whether they elicited wing spreading (WS) and whether the pair copulated during the recording period.  $n=467, 126, 356, 102$ .

**c,d**, Latency of WS from pulse train onset (**c**) and the length of pulse train after WS onset (**d**), respectively, separated by whether the pair copulated during the recording period. In (**d**), the non-parametric two-sided Mann-Whitney U test is used to test for statistical difference between the two groups.  $n=126, 102$ .

**e**, Length of pulse trains in pairs with intact females, separated by whether they elicited WS, and in pairs with WC females. Only data from pairs that did not copulate during the recording period are shown.  $n=410, 713, 119$ .

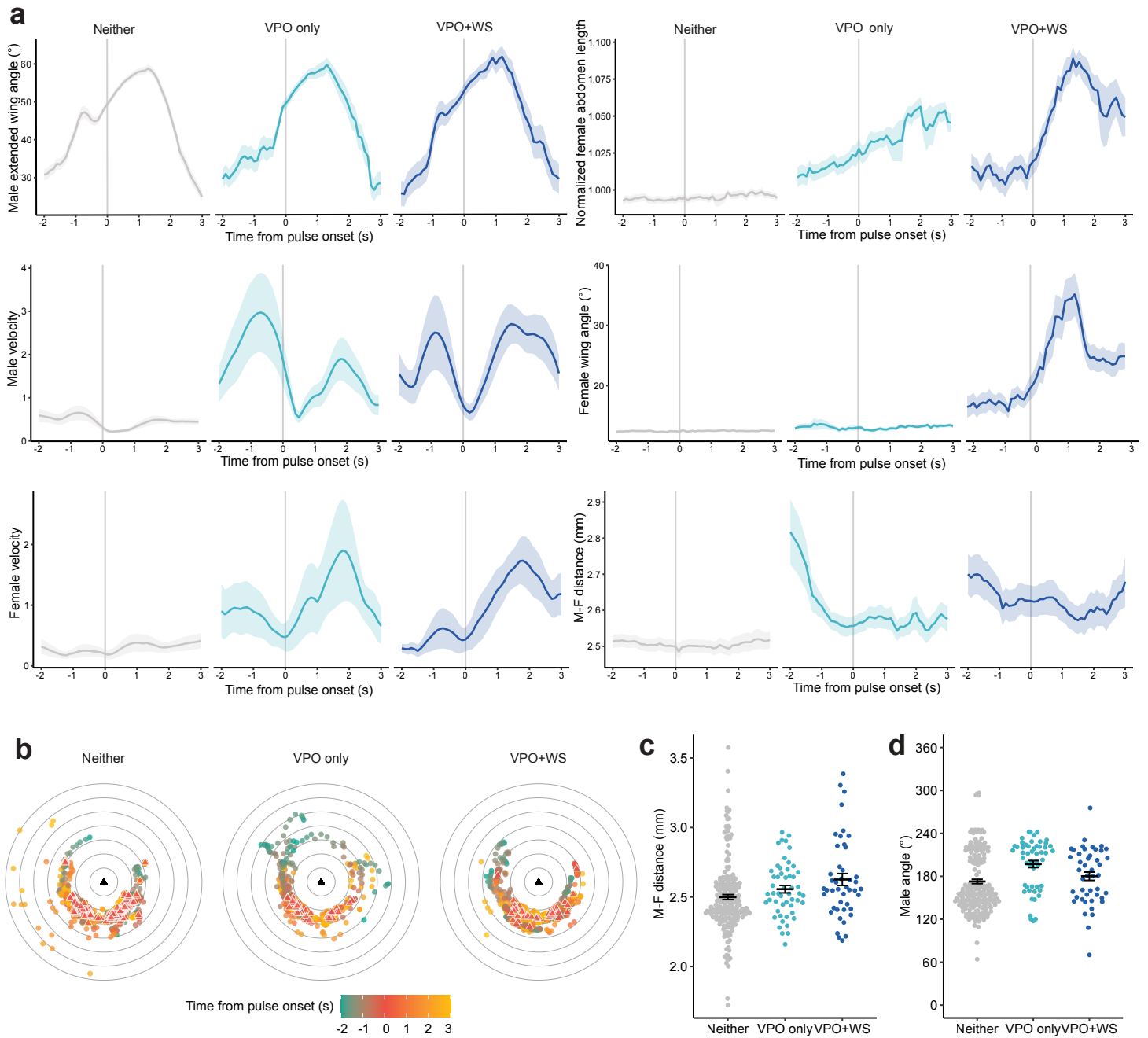
**f**, Number of pulse trains per minute that males produced when paired with intact or WC females. None of the pairs copulated during the recording period.  $n=16, 21$ .

**g**, Probability of observing WS in response to a male pulse train.  $n=16$

**h**, Mean length of pulse trains in pairs with intact females, separated by whether they elicited WS, and in pairs with WC females.  $n=16, 6, 21$ .

**i**, Length of pulse trains in pairs with intact females, separated by whether they elicited WS, and in pairs with WC females. Four outliers with pulse trains  $>18s$  are removed to facilitate clearer data visualization.  $n=395, 32, 724$ .

Figure shows conspecific courtship between *D. santomea* females and males (**a-e**) and heterospecific courtship between *D. santomea* females and *D. yakuba* males (**f-i**). Error bars show mean  $\pm$  SEM. Unless otherwise specified, statistical significance was tested with two-sided ANOVA on linear models (**a,f**), or linear mixed models using pair identity as a random effect (**b,c,e,h,i**), with post hoc Tukey test. Source data are provided as a Source Data file.



**Supplementary Fig. 3: Female and male behavioral parameters during pulse events.**

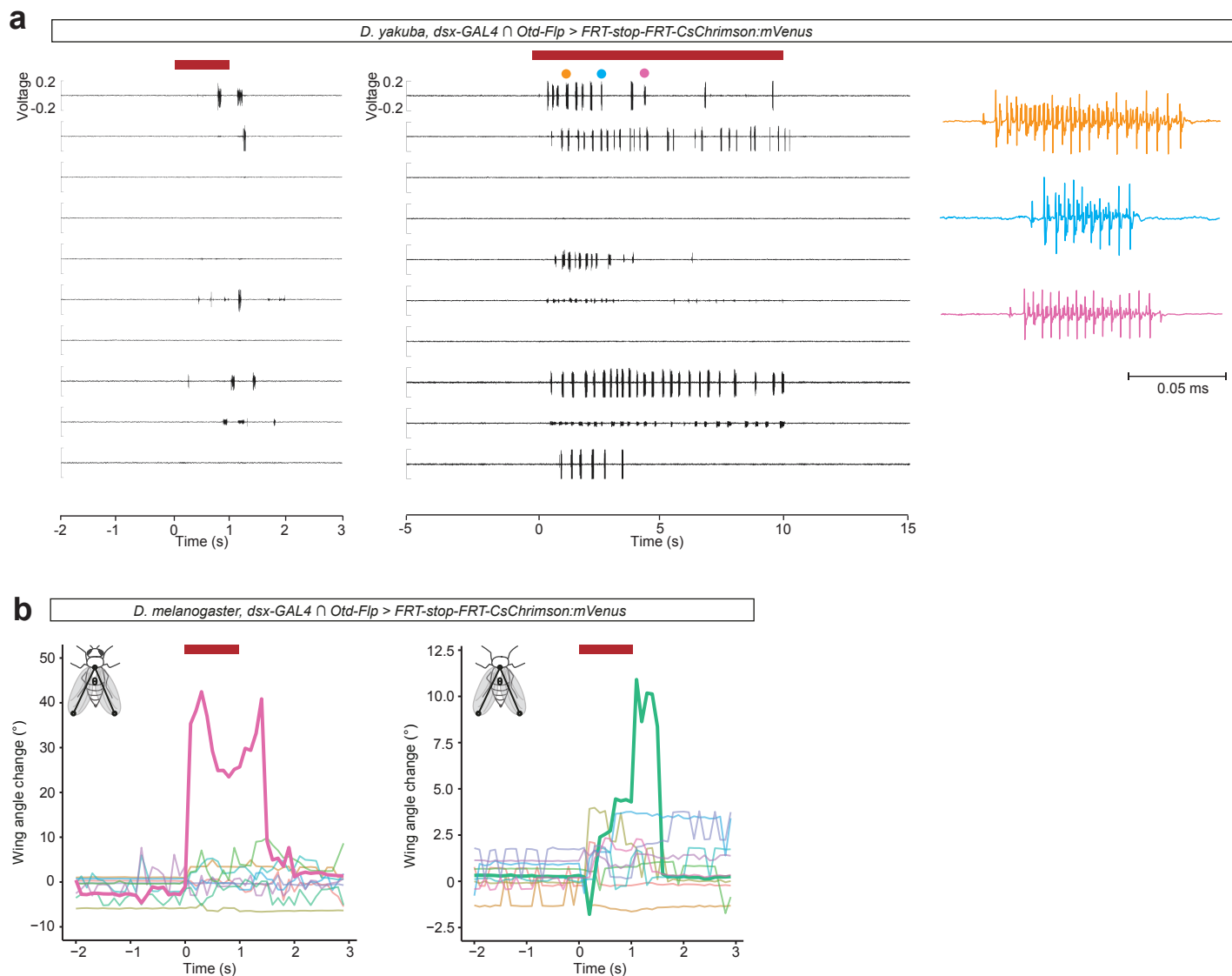
**a**, Mean male extended wing angle, male velocity, female velocity, normalized female abdomen length, female wing angle, and distance between male and female thoraces, separated by event type. Pulse onset is marked with a vertical gray line. Shaded areas represent the SEM.

**b**, Male position in female-centered coordinates during all pulse events, separated by event type. The female is represented by a triangle in the center, with the head pointing up. Each ring represents 1 mm. Male position at pulse onset is marked as a red triangle.

**c**, Distance between male and female thoraces at pulse onset compared across all event types.

**d**, Male angle relative to the female body axis compared across all event types. At 180°, the male is directly behind the female. Error bars show mean±SEM. n=207 (Neither), 52 (VPO only), 45 (VPO+WS) events from 13 females. Source data are provided as a Source Data file.

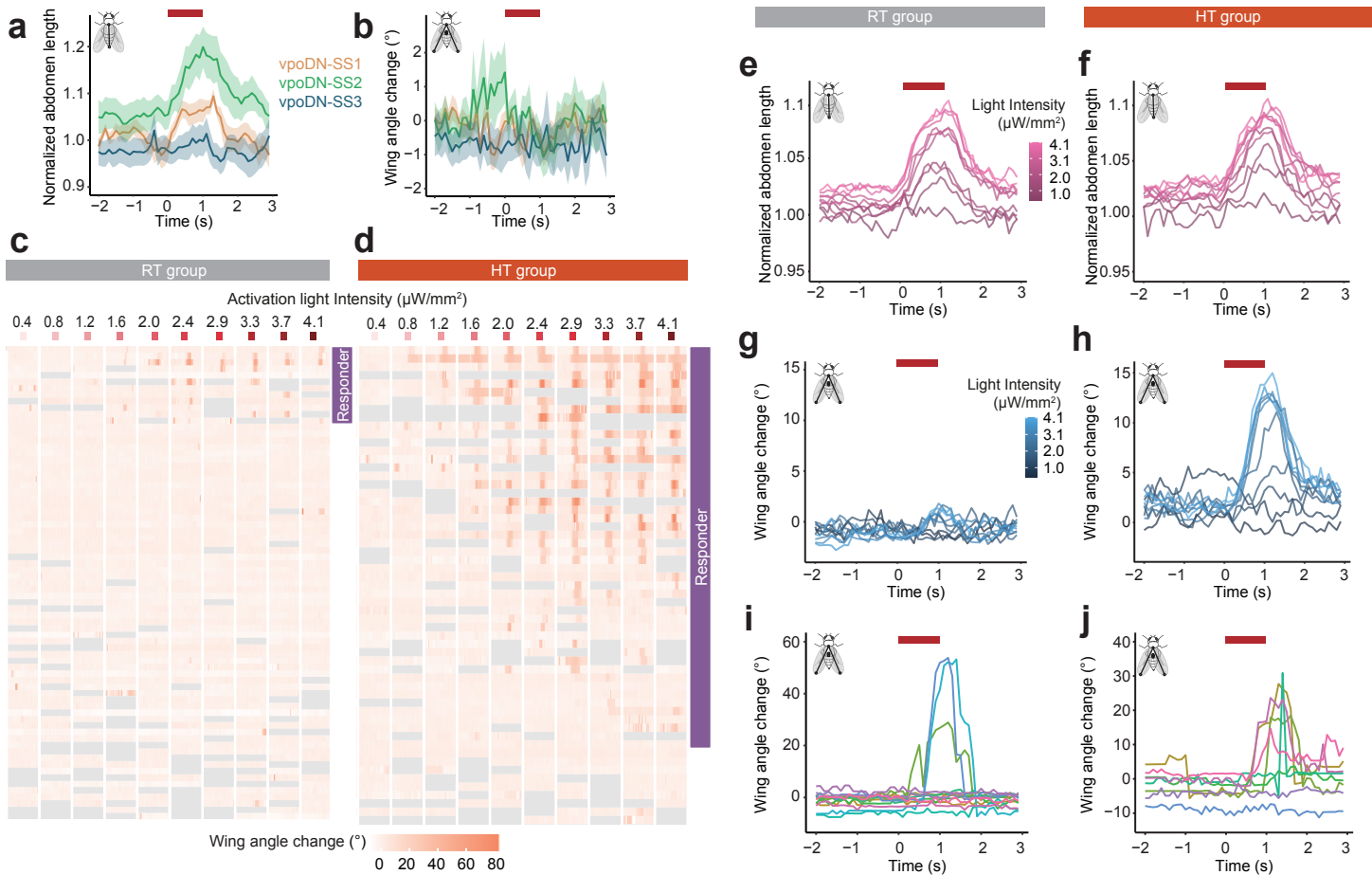




**Supplementary Fig. 4: Additional behavioral phenotypes of activating brain *dsx* neurons in *D. yakuba* and *D. melanogaster*.**

**a**, Audio traces upon activating *dsx* brain neurons in decapitated *D. yakuba* females using a 1s (left) or a 10s (right) activation scheme with a light intensity of of  $4 \mu\text{W}/\text{mm}^2$ . Each row represents one individual. Activation window is denoted by red bars. Three examples of female song events (right) show the production of polycyclic signals with stereotypic waveforms in variable lengths.

**b**, Wing angle change in intact *D. melanogaster* females at  $1.6 \mu\text{W}/\text{mm}^2$ , and decapitated females at  $0.8 \mu\text{W}/\text{mm}^2$ . Activation window is denoted by red bars. Each line with a different color represents one individual. Individuals showing wing spreading response in this activation window are highlighted with thicker lines.  $n=10$  (intact), 10 (decapitated). Source data are provided as a Source Data file.



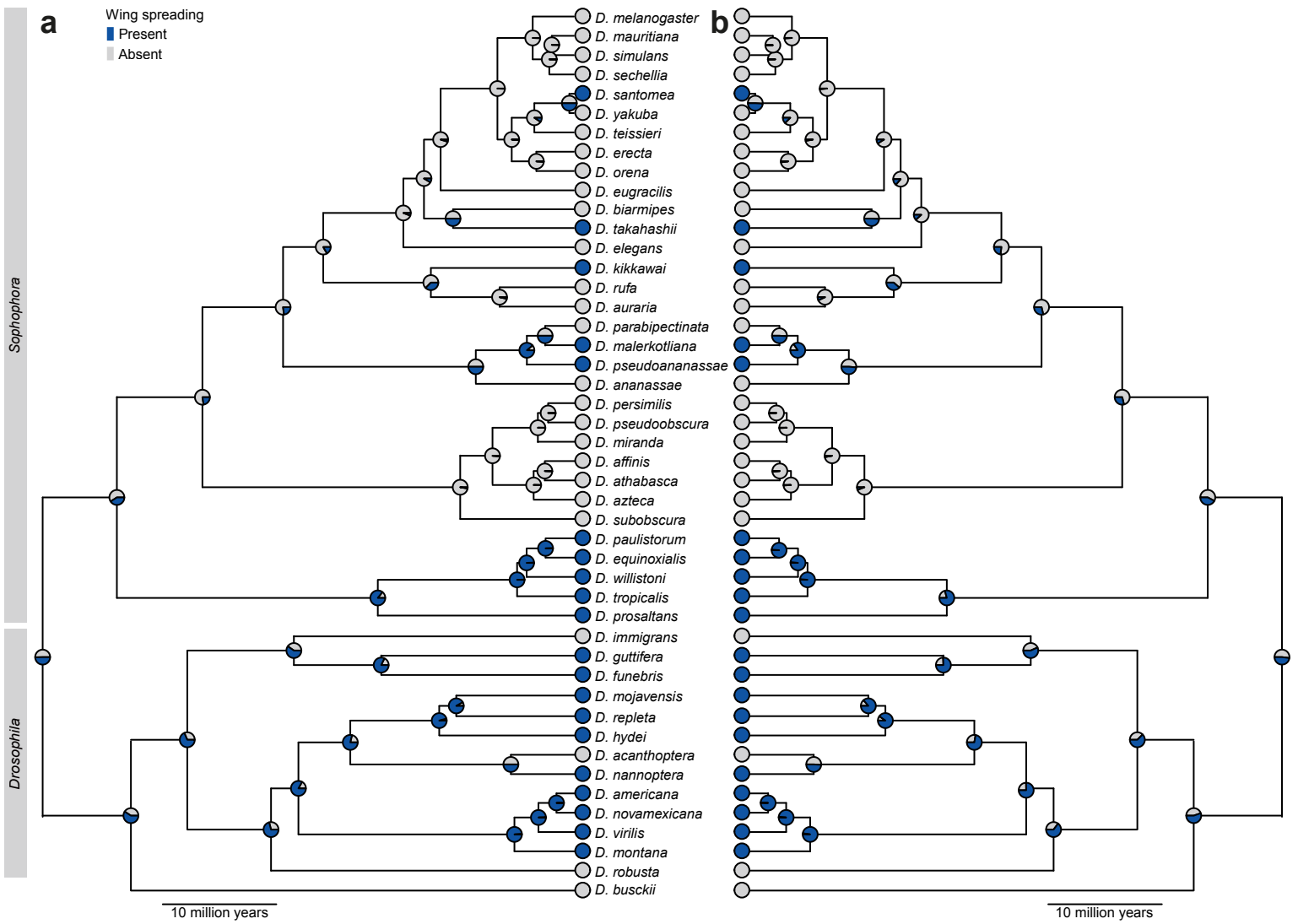
**Supplementary Fig. 5: Additional behavioral analyses associated with Fig. 5 showing developmental temperature-dependent modulation of wing spreading phenotype upon vpoDN activation.**

**a,b**, Mean normalized abdominal length (**a**) and wing angle change (**b**) of *D. melanogaster* *vpoDN-SS1*, *vpoDN-SS2* or *vpoDN-SS3* > *UAS-CsChrimson:mVenus* females at 4.1  $\mu\text{W}/\text{mm}^2$ . Activation window is denoted by red bars. Shaded areas represent the SEM. Inset diagrams illustrate how abdomen lengths or wing angles were measured.  $n=9$  (*vpoDN-SS1*), 11 (*vpoDN-SS2*), 11 (*vpoDN-SS3*).

**c,d**, Wing angle changes of *D. melanogaster* *vpoDN-SS2* > *UAS-CsChrimson:mVenus* females from RT group (**c**) and HT group (**d**) across 10 activation bouts with intensity from 0.4 to 4.1  $\mu\text{W}/\text{mm}^2$ . Each row represents one individual. Each column represents a 5-second period centered at 1-second activation window (red bar) with light intensity listed above. Frames with low tracking quality are shown in gray. The manually scored responders are noted on the right side.  $n=73$  (RT group), 57 (HT group).

**e-h**, Mean normalized abdominal lengths (**e,f**) and wing angles (**g,h**) of *D. melanogaster* *vpoDN-SS2* > *UAS-CsChrimson:mVenus* females from RT group (**e,g**) and HT group (**f,h**) at different activation intensities denoted by colors. Activation window is denoted by red bars.  $n=91$  (RT group), 80 (HT group).

**i,j**, Wing angle changes of *D. melanogaster* *vpoDN-SS2* > *UAS-CsChrimson:mVenus* females from RT group (**i**) and HT group (**j**) at 3.3  $\mu\text{W}/\text{mm}^2$ . Ten individuals were randomly selected in the plot and each line represents one individual. Activation window is denoted by red bars.  $n=13$  (**i**), 8 (**j**). Source data are provided as a Source Data file.



**Supplementary Fig. 6: Ancestral state reconstruction of wing spreading on an expanded phylogenetic tree.**

**a**, Maximum likelihood inference of the ancestral states.

**b**, Bayesian inference of the ancestral states.

Phylogeny is based on <sup>30,32</sup>. Leaf nodes: whether wing spreading is observed in each species based on this study and Spieth 1952<sup>20</sup>.

Pie charts of the Internal nodes represent the inferred probabilities of either state (**a**) and the posterior probabilities of either state (**b**).

Blue: ancestral state with the presence of wing spreading; gray: ancestral state with absence of wing spreading. VPO was observed in all species in this phylogeny<sup>20</sup>.

**Supplementary Table 1: *Drosophila* strains used in this study.**

<b>Figure</b>	<b>Species</b>	<b>Strains</b>
Figs. 1a-f, 2, 3, 6 Extended Data Figs. 1-3	<i>D. santomea</i>	STO4
Fig. 1g	<i>D. santomea</i>	18CAR05-10
Fig. 1g	<i>D. santomea</i>	18TRNE01-05
Fig. 1g	<i>D. santomea</i>	Q1-02
Figs. 2a, 6 Extended Data Fig. 2f-i	<i>D. yakuba</i>	14021-0261.02
Fig. 1g	<i>D. yakuba</i>	3-41
Fig. 1g	<i>D. yakuba</i>	4-72
Fig. 1g	<i>D. yakuba</i>	1-03
Fig. 1g	<i>D. yakuba</i>	2-0F11
Figs. 1g, 2a, 5h,i, 6	<i>D.melanogaster</i>	Canton S
Figs. 1g, 6	<i>D. simulans</i>	sim5
Figs. 1g, 6	<i>D. teissieri</i>	14021-0257.01
Figs. 1g, 6	<i>D. erecta</i>	14021-0224.01
Fig. 4a-i	<i>D. santomea</i>	sanw; ; Otd-Flp (2253), <i>dsx</i> -GAL4/FRT-stop-FRT-CsChrimson:mVenus (2253)
Fig. 4a-i	<i>D.melanogaster</i>	w1118; Otd-Flp (attP40)/+; <i>dsx</i> -GAL4/FRT-stop-FRT-CsChrimson:mVenus (vk5)
Extended Data Fig. 4a,b	<i>D. yakuba</i>	yakw; FRT-stop-FRT-CsChrimson:mVenus (2180)/+; <i>dsx</i> -GAL4/Otd-Flp (2285)
Fig. 4a-i	<i>D. yakuba</i>	yakw; FRT-stop-FRT-CsChrimson:mVenus (2180)/+; <i>dsx</i> -GAL4/Otd-Flp (2285)
Extended Data Fig. 4c,d	<i>D.melanogaster</i>	vpoDN-SS2: 20xUAS-CsChrimson-mVenus (attP18)/w1118; 45670-AD(p40)/Cyo; 52F12-DBD(p2)=ss50795
Fig. 5a-h	<i>D.melanogaster</i>	vpoDN-SS2: 20xUAS-CsChrimson-mVenus (attP18)/w1118; 45670-AD(p40)/Cyo; 52F12-DBD(p2)=ss50795
Extended Data Fig. 5a-j	<i>D.melanogaster</i>	vpoDN-SS2: 20xUAS-CsChrimson-mVenus (attP18)/w1118; 45670-AD(p40)/Cyo; 52F12-DBD(p2)=ss50795
Extended Data Fig. 5a,b	<i>D.melanogaster</i>	vpoDN-SS1: 20xUAS-CsChrimson-mVenus (attP18)/w1118; 31D07-AD(p40)/Cyo; 52F12-DBD(p2)=ss50200
Extended Data fig. 5a,b	<i>D.melanogaster</i>	vpoDN-SS3: 20xUAS-CsChrimson-mVenus (attP18)/w1118;45670-AD(p40)/Cyo;10A09-DBD(p2)=ss53451
Fig. 6	<i>D. eugracilis</i>	14026-0451.02
Fig. 6	<i>D. lucipennis</i>	unknown
Fig. 6	<i>D. biarmipes</i>	G#224
Fig. 6	<i>D. takahashii</i>	unknown
Fig. 6	<i>D. elegans</i>	unknown
Fig. 6	<i>D. gunungola</i>	sk
Fig. 6	<i>D. kikkawai</i>	14028-05161.14
Fig. 6	<i>D. parabiptinata</i>	VT04-70 Vietnam
Fig. 6	<i>D. malerkotliana</i>	C1Z19-L9
Fig. 6	<i>D. ananassae</i>	14024-0371.13
Fig. 6	<i>D. biptinata</i>	THT 08 Taiwan
Fig. 6	<i>D. pseudoananassae</i>	R186 Puerto Princessa
Fig. 6	<i>D. pseudoobscura</i>	14022-0121.94
Fig. 6	<i>D. willistoni</i>	14030-0814.24
Fig. 6	<i>D. ezoana</i>	15010-0971.00
Fig. 6	<i>D. mojavnensis wrightleyi</i>	15081-1352.22
Fig. 6	<i>D. mercatorum</i>	unknown

## Supplementary files

**Supplementary Movie 1:** Exemplar events of wing spreading in wildtype *D. santomea* pairs.

**Supplementary Movie 2:** Typical behavioral phenotypes of activating *dsx* brain neurons in intact and decapitated *D. santomea*, *D. melanogaster*, and *D. yakuba*.

**Supplementary Movie 3:** Female singing induced by activating *dsx* brain neurons in *D. yakuba*.

**Supplementary Movie 4:** Occasional wing spreading induced by activating *dsx* brain neurons in *D. melanogaster*.

**Supplementary Movie 5:** Occasional wing spreading induced by activating vpoDN in *D. melanogaster*.

**Supplementary Movie 6:** Exemplar events of wing spreading in wildtype *D. melanogaster* pairs.

**Supplementary Movie 7:** Exemplar events of wing spreading in other species (*D. takahashii*, *D. kikkawai*, *D. malerkotliana*, *D. pseudoananassae*, *D. willistoni*, *D. mojavensis* and *D. mercatorum*) during courtship or before copulation.

**Supplementary Data 1:** Data and scripts used in data analysis.